nature biomedical engineering
SUPPLEMENTARY INFORMATION
DOI: 10.1038/s41551-017-0116-7
In the format provided by the authors and unedited.

Iron oxide nanoclusters for T_1 magnetic resonance imaging of non-human primates

Yang Lu[1,2,3], Yun-Jun Xu[4], Guo-bing Zhang[5], Daishun Ling[6,7], Ming-quan Wang[5], Yong Zhou[8], Ya-Dong Wu[3], Tao Wu[8], Michael J. Hackett[1,2], Byung Hyo Kim[1,2], Hogeun Chang[1,2], Jonghoon Kim[1,2], Xin-Tian Hu[9], Liang Dong[3], Nohyun Lee[1,2,10], Fangyuan Li[6,7], Jia-Cai He[8], Li Zhang[5], Hui-Qin Wen[5], Bo Yang[6], Seung Hong Choi[1,11]*, Taeghwan Hyeon[1,2]* and Duo-Hong Zou[8,12]*

[1]Center for Nanoparticle Research, Institute for Basic Science (IBS), Seoul 08826, Republic of Korea. [2]School of Chemical and Biological Engineering, and Institute of Chemical Processes, Seoul National University, Seoul 08826, Republic of Korea. [3]School of Chemistry and Chemical Engineering, Hefei University of Technology, Hefei 230009, China. [4]Department of Radiology, Anhui Provincial Hospital, Hefei 230001, China. [5]The First Affiliated Hospital of Anhui Medical University, Anhui Medical University, Hefei 230022, China. [6]Zhejiang Province Key Laboratory of Anti-Cancer Drug Research, College of Pharmaceutical Sciences, Zhejiang University, Hangzhou 310058, China. [7]Key Laboratory of Biomedical Engineering of the Ministry of Education, College of Biomedical Engineering and Instrument Science, Zhejiang University, Hangzhou 310058, China. [8]Department of Dental Implant Centre, Stomatologic Hospital and College, Anhui Medical University, Key Laboratory of Oral Diseases Research of Anhui Province, Hefei 230032, China. [9]Kunming Institute of Zoology, Chinese Academy of Sciences, Kunming 650223, China. [10]School of Advanced Materials Engineering, Kookmin University, Seoul 02727, Republic of Korea. [11]Department of Radiology, Seoul National University Hospital, and the Institute of Radiation Medicine, Medical Research Center, Seoul National University, Seoul 03080, Republic of Korea. [12]Second Dental Clinic, Ninth People's Hospital, Shanghai Jiao Tong University, School of Medicine, Shanghai Key Laboratory of Stomatology, National Clinical Research Center of Stomatology, Shanghai 200001, P. R. China. Yang Lu, Yun-Jun Xu, Guo-bing Zhang and Daishun Ling contributed equally to this work. *e-mail: verocay@snuh.org; thyeon@snu.ac.kr; zdhyy@ahmu.edu.cn

Supplementary Information

Iron oxide nanoclusters for T_1 MRI of nonhuman primates

Yang Lu[1,2,3]†, Yun-Jun Xu[4]†, Guo-bing Zhang[5]†, Daishun Ling[6,7]†, Ming-quan Wang[5], Yong Zhou[8], Ya-Dong Wu[3], Tao Wu[8], Michael J. Hackett[1,2], Byung Hyo Kim[1,2], Hogeun Chang[1,2], Jonghoon Kim[1,2], Xin-Tian Hu[9], Liang Dong[3], Nohyun Lee[1,2,10], Fangyuan Li[6,7], Jia-Cai He[8], Li Zhang[5], Hui-Qin Wen[5], Bo Yang[6], Seung Hong Choi[1,11]*, Taeghwan Hyeon[1,2]* and Duo-Hong Zou[8]*

[1]Center for Nanoparticle Research, Institute for Basic Science (IBS), Seoul 08826, Republic of Korea.
[2]School of Chemical and Biological Engineering, and Institute of Chemical Processes, Seoul National University, Seoul 08826, Republic of Korea
[3]School of Chemistry and Chemical Engineering, Hefei University of Technology, Hefei, 230009, China.
[4]Department of Radiology, Anhui Provincial Hospital, Hefei 230001, China.
[5]The First Affiliated Hospital of Anhui Medical University, Anhui Medical University, Hefei 230022, China.
[6]Zhejiang Province Key Laboratory of Anti-Cancer Drug Research, College of Pharmaceutical Sciences, Zhejiang University, Hangzhou 310058, China.
[7]Key Laboratory of Biomedical Engineering of the Ministry of Education, College of Biomedical Engineering & Instrument Science, Zhejiang University, Hangzhou 310058, China.
[8]Department of Dental Implant Centre, Stomatologic Hospital & College, Anhui Medical University, Key Laboratory of Oral Diseases Research of Anhui Province, Hefei 230032, China.
[9]Kunming Institute of Zoology, Chinese Academy of Sciences, Kunming 650223, China.
[10]School of Advanced Materials Engineering, Kookmin University, Seoul 02727, Republic of Korea.
[11]Department of Radiology, Seoul National University Hospital, and the Institute of Radiation Medicine, Medical Research Center, Seoul National University, Seoul 03080, Republic of Korea.

† These authors contributed equally to this work.
Correspondence should be addressed to: *e-mail: thyeon@snu.ac.kr, zdhyy@ahmu.edu.cn, verocay@snuh.org

Table of Contents

Detailed MRI procedures.

MRA and perfusion weighted imaging (PWI). All MRI scans were performed on a 3.0 T clinical MR scanner (Trio Tim, Siemens, Germany) equipped with head, neck and body coils. FLASH-3D sequence was employed for the MRA of beagle dogs and macaque monkeys, and bolus injection of PEG-IONCs was performed through the vein of upper limb at a dose of 10 mg per kg body weight at a rate of 4 mL per second using an MR-compatible high-pressure mechanical injector (OptiStar LE, Mallinckrodt, US). During the MRI, respiration was monitored for real-time tracking of the anesthetic condition of the animals. Turbo Spin Echo (TSE) sequence and FLASH-2D sequence were employed for the T_2-weighted and T_1-weighted imaging, respectively, of the ischemic brain. Spin Echo diffusion-weighed imaging (DWI) was obtained to confirm the cerebral infarction. Echo planar imaging (EPI) sequence was employed for the PWI. Susceptibility weighted imaging (SWI) was also obtained to evaluate the venous structures and PEG-IONCs-enhanced imaging.

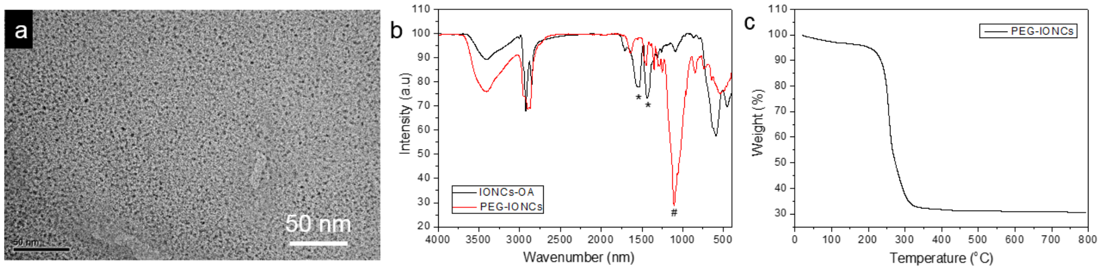

Figure S1. Supplementary characterization of PEG-IONCs. (a) TEM image of IONCs. (b) Carboxylate bands (1430 cm^{-1} and 1530 cm^{-1}, marked with *) corresponding to oleic acid are present in the FT-IR spectrum of hydrophobic iron oxide nanoclusters (IONCs), and carbon-oxygen single bond (1106 cm^{-1}, marked with #) corresponding to PEG molecules is present in the FT-IR spectrum of hydrophilic PEG-stabilized iron oxide nanoclusters (PEG-IONCs). (c) The weight loss in PEG-IONCs is measured to be around 68% in TGA data, which indicates the large amount of PEG molecules serving as surface ligands in PEG-IONCs to prevent the aggregation of IONCs during the ligand exchange process.

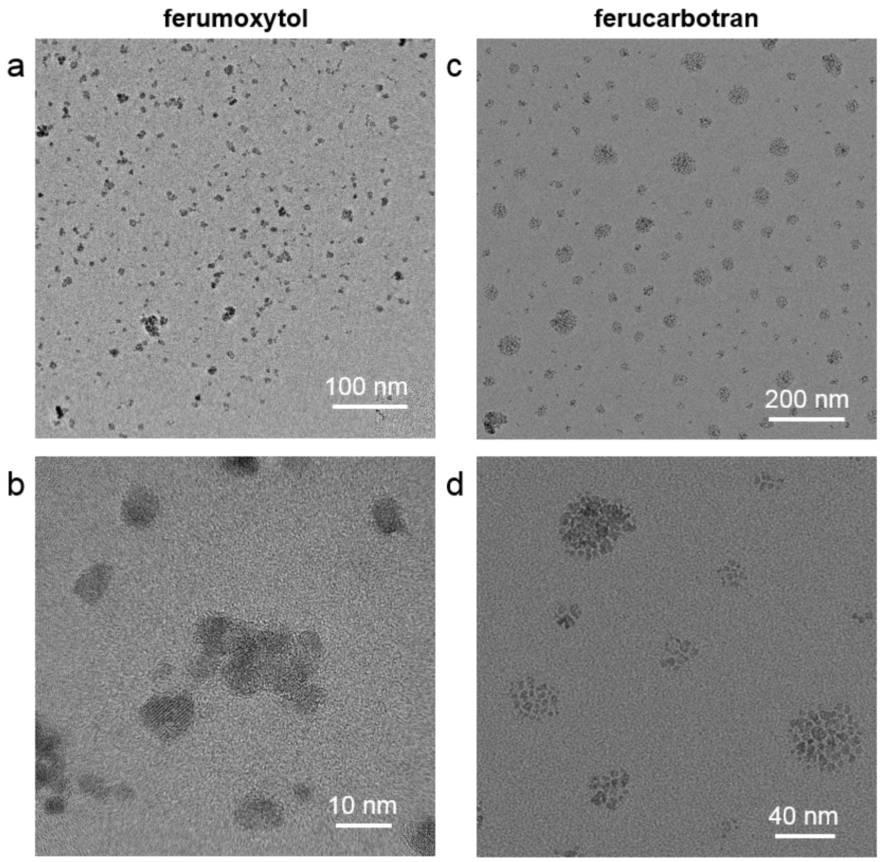

Figure S2. TEM images of (a, b) ferumoxytol and (c, d) ferucarbotran. The core sizes of (a, b) ferumoxytol and (c, d) ferucarbotran are about 7 nm and 5 nm, respectively, which are in agreement with the previous reports (*J. Magn. Reson. Imaging* **21**, 46 (2005); *Chem. Mater.* **22**, 1739 (2010)). Furthermore, several particles are aggregated into clusters, so the hydrodynamic size is much larger than the individual core size.

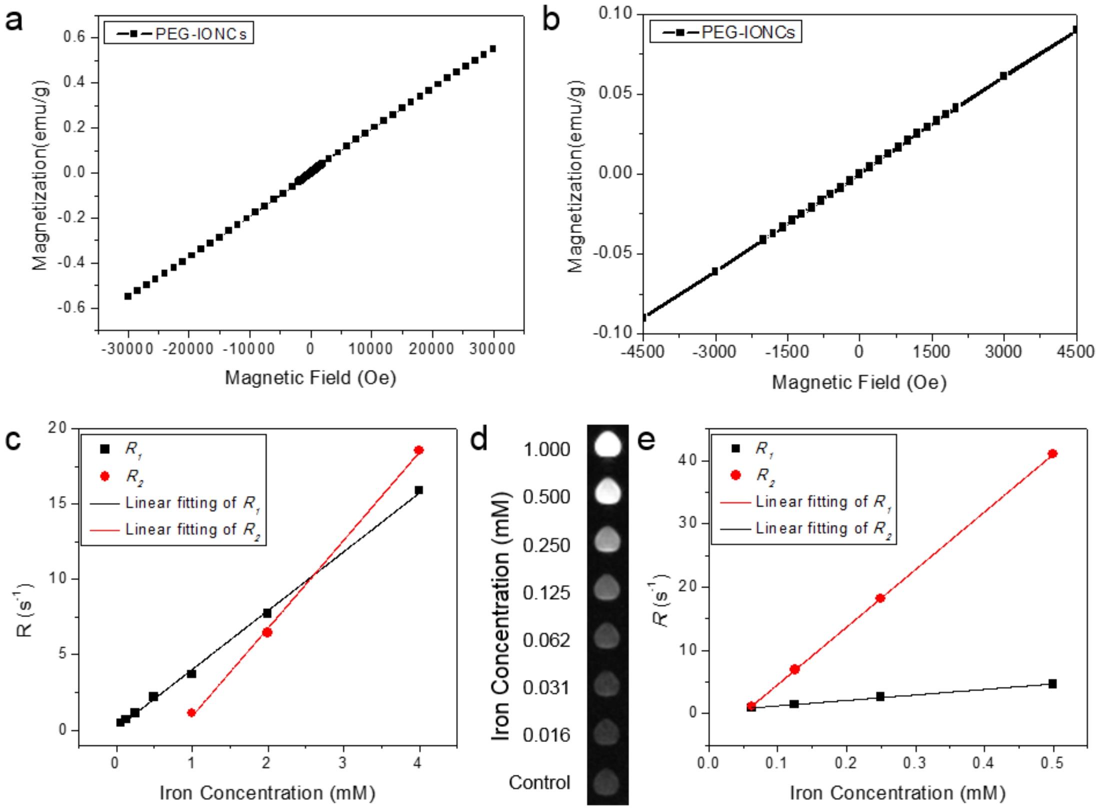

Figure S3. Magnetic and MR characterization of PEG-IONCs. (a, b) M-H curve at 300K between -3 to 3 T and enlarged M-H curve show the paramagnetic characteristics of hydrophilic PEG-IONCs. (c) Plot of resistivity over iron concentration and (d) T_1-weighted MR phantom of IONCs. (e) Plot of resistivity over iron concentration of ferumoxytol.

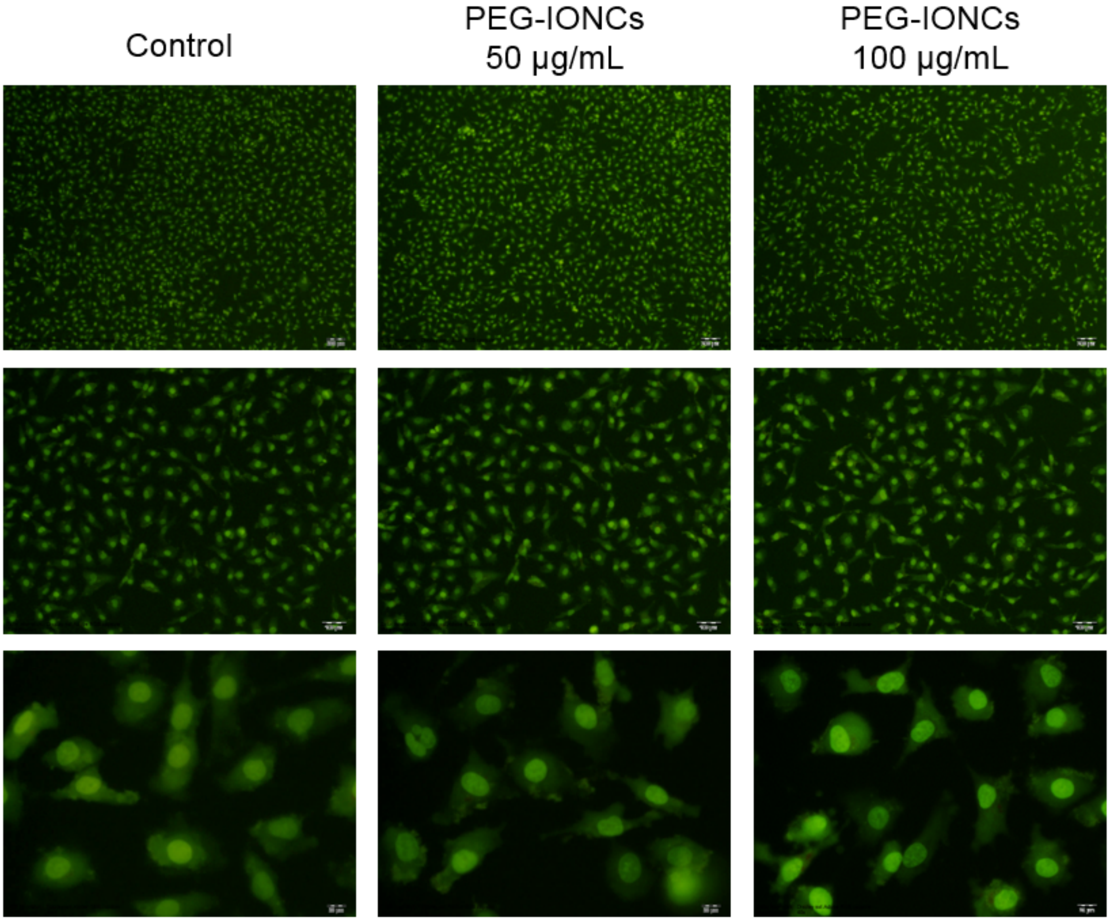

Figure S4. After exposure to 50 and 100 μg/mL of PEG-IONCs, cytotoxicity evaluation was performed on human umbilical vein endothelial cells (HUVEC) through AO-EB staining. AO stains live cells while EB stains dead cells. No obvious cellular death was induced by PEG-IONCs.

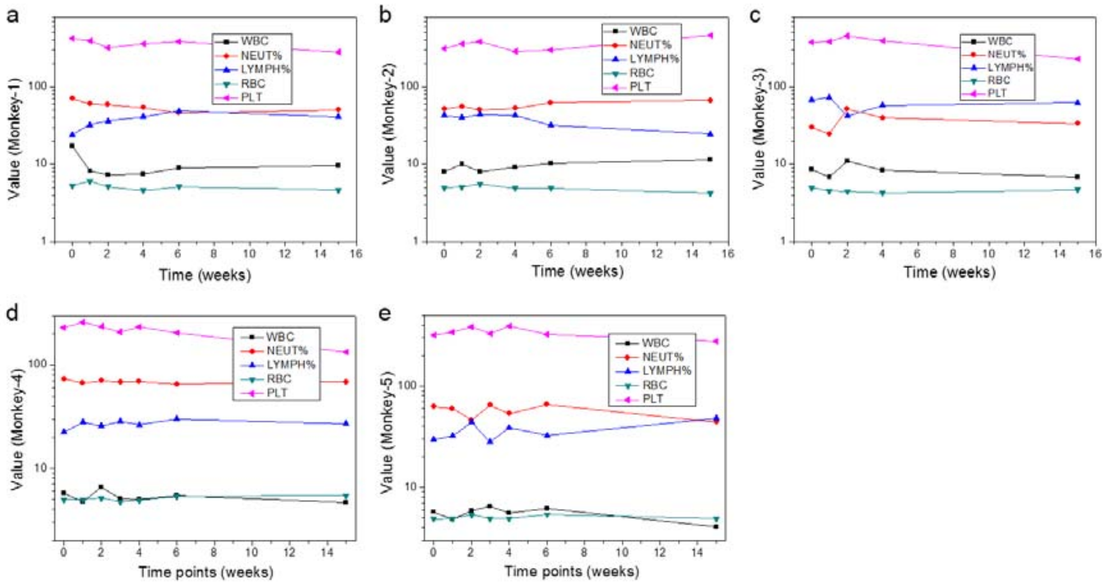

Figure S5. Hematological evaluation after the intravenous bolus injection of PEG-IONCs on monkeys. Different from small animals, the whole blood of monkey could be collected at a series of time points. The hematological values before the injection of PEG-IONCs are considered to be the control values to evaluate the hematological effect of PEG-IONCs on monkeys.

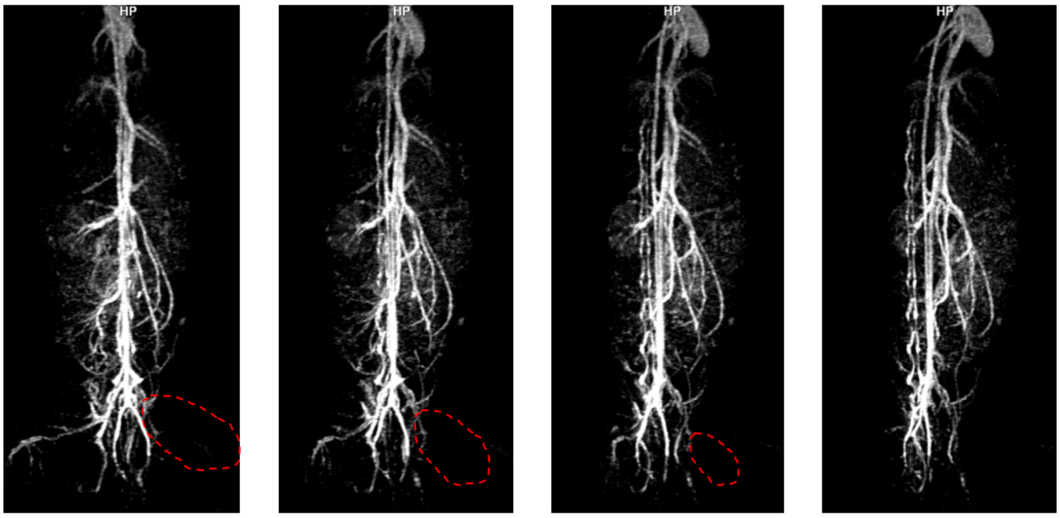

Figure S6. MRA diagnosis of right lower limb ischemia on rabbit using PEG-IONCs from different angles of view, and the disappeared right lower limb vessel is circled by dashed red line. Spinal vessels also appear in these images.

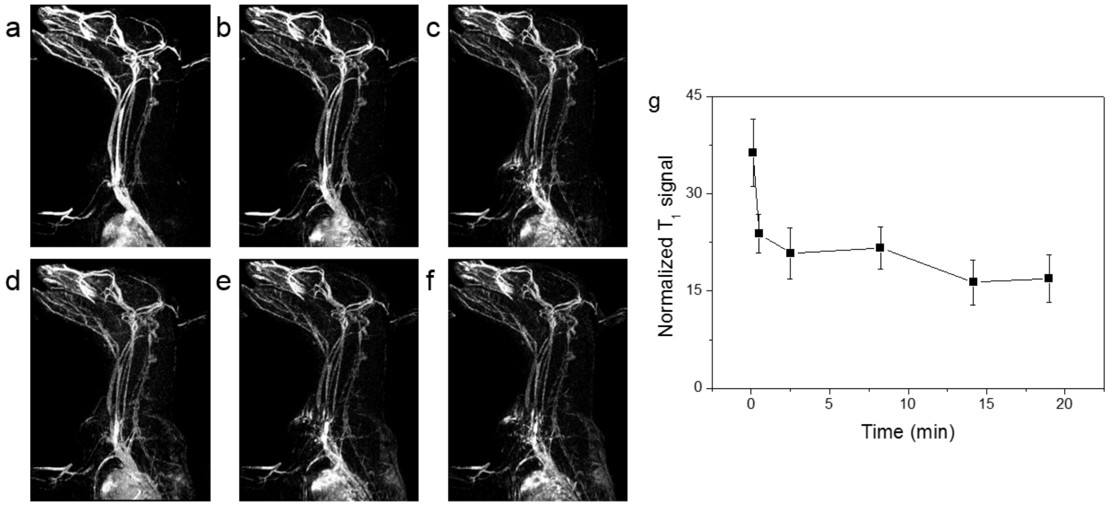

Figure S7. Dynamic MRA images of upper body in beagle dog after the bolus injection of PEG-IONCs were collected at a series of time points from (a) 8 s, (b) 30 s, (c) 2 min 30 s, (d) 8 min 15 s, (e) 14 min 10 s, to (f) 19 min. The corresponding normalized T_1 signal intensities in the heart were measured (selected area is 0.69 cm^2) (g). In the first 30 s, due to the high concentration of contrast agents derived from bolus injection, the signal of vessels is much higher. After 2 minutes, no obvious decrease of the T_1 signal is observed, indicating the PEG-IONCs-mediated bright signal of blood vessels is maintained, which is consistent with the observations in MRA (c)-(f). This long-term contrast ability of PEG-IONCs in vivo is in a strong contrast with a quick clearance of gadolinium-based contrast agents (GBCAs).

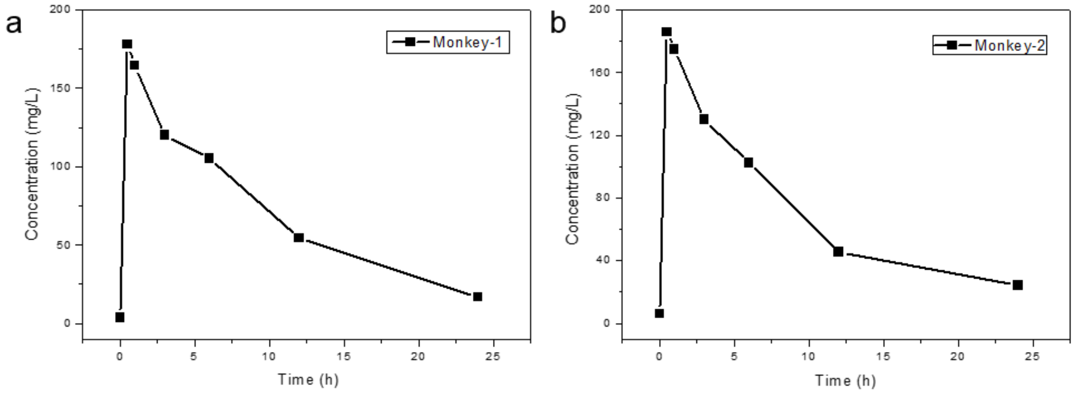

Figure S8. Blood plasma concentration on two random selected healthy monkeys after intravenous injection at the dose of 10 mg/kg bw.

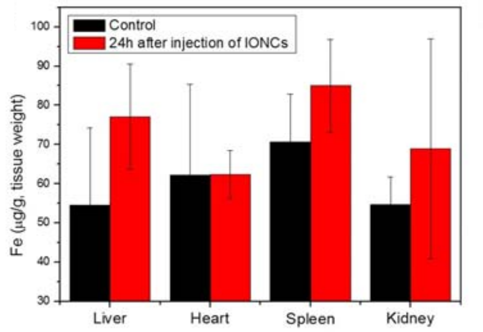

Figure S9. Distribution of iron in heart and major metabolic tissues including liver, spleen and kidney 24 hours after intravenous injection at the dose of 10 mg/kg bw (ICR mice, female, 20-25g bw, n=4-6).

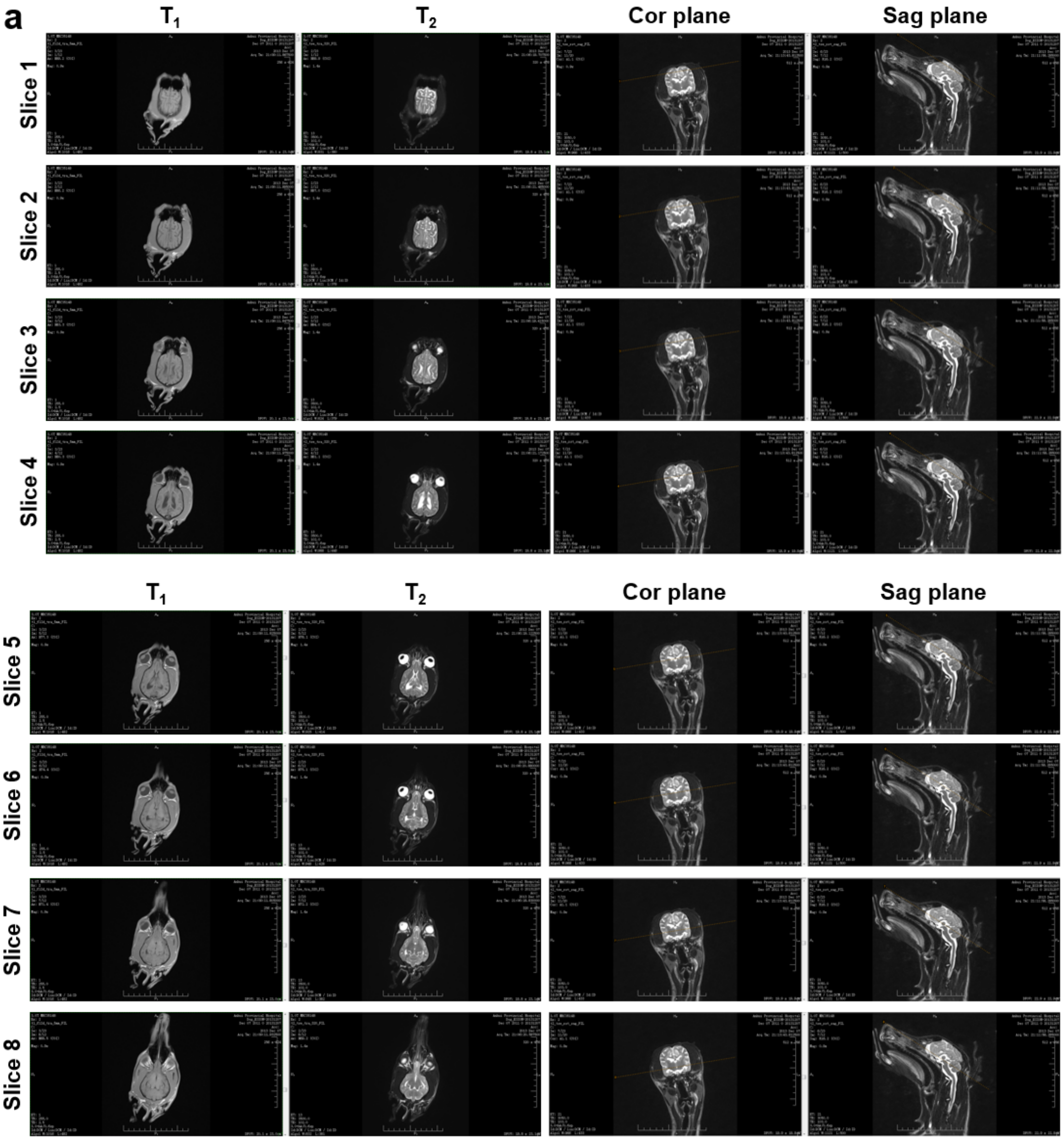
a
T1
T2
Cor plane
Sag plane
Slice 1
Slice 2
Slice 3
Slice 4
Slice 5
Slice 6
Slice 7
Slice 8

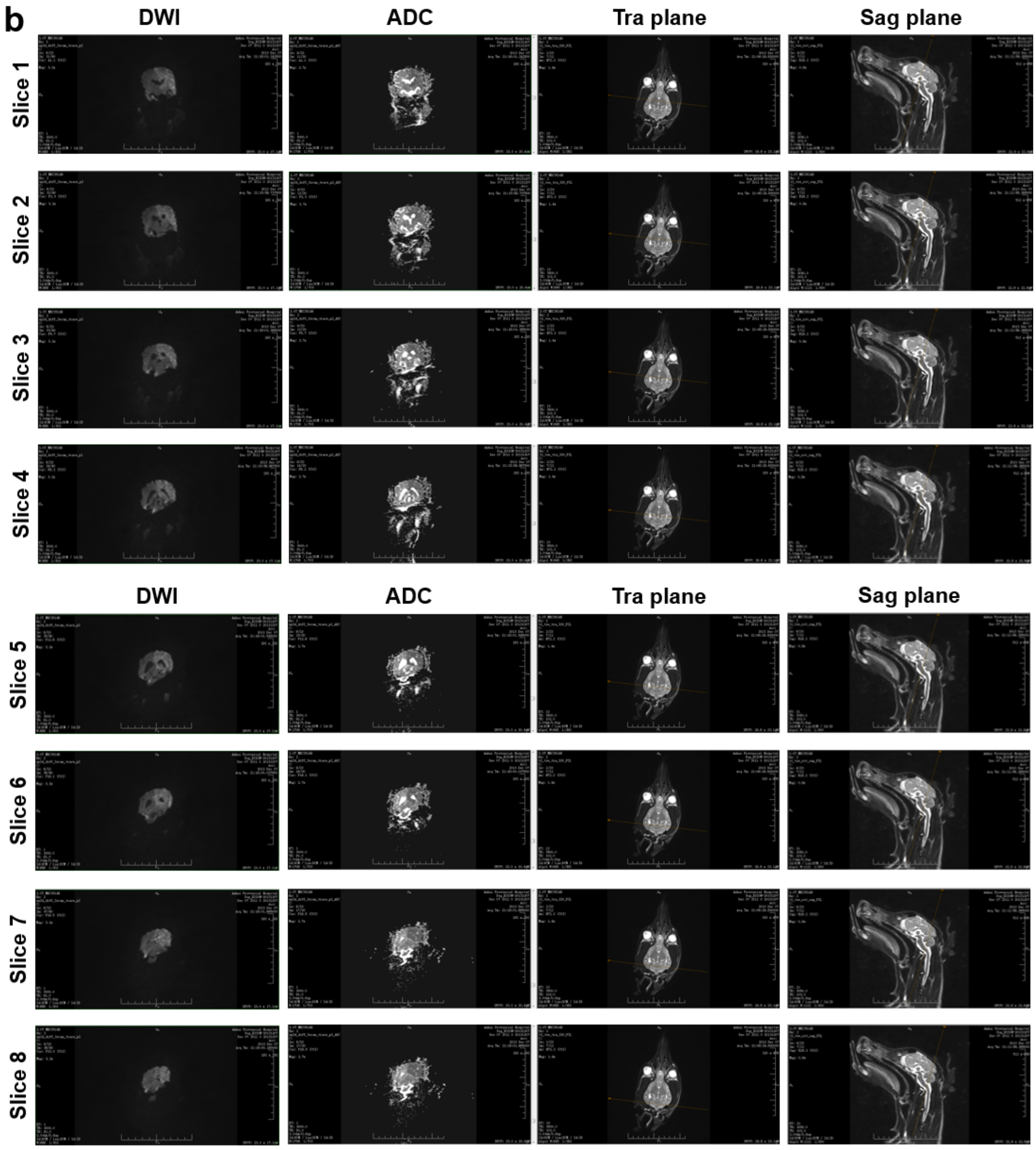

Figure S10. MRI series of a beagle dog with left cerebral ischaemia. (a) T_1-weighted, T_2-weighted and relative coronal (Cor) and sagittal (Sag) plane and (b) diffusion-weighted MR imaging (DWI) images and relative transverse (Tra) and sagittal (Sag) plane.

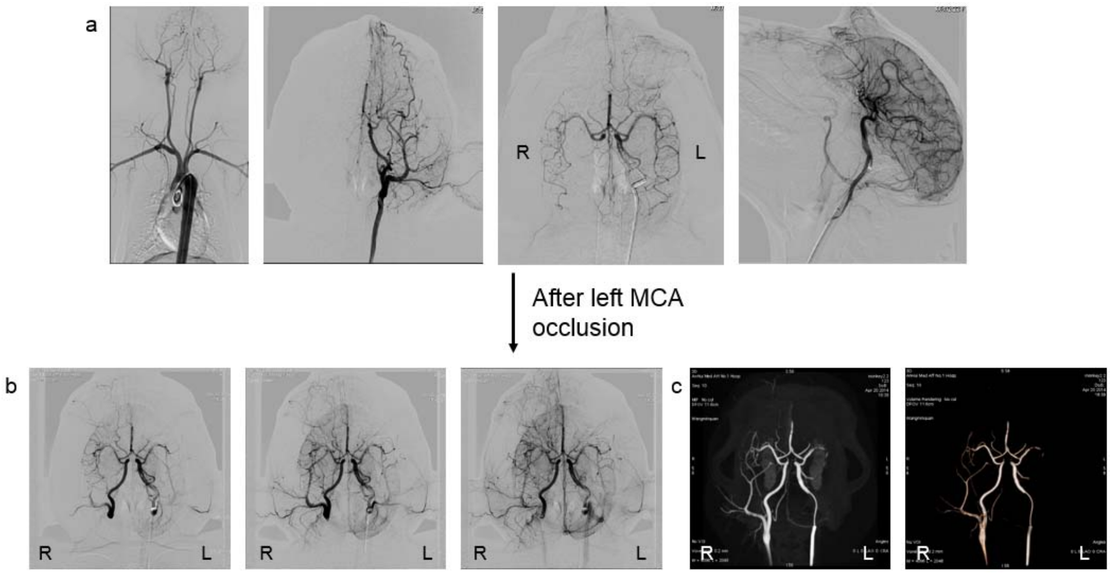

Figure S11. Digital subtraction angiography (DSA) images (a) before and (b) after the interventional procedure on monkey, indicating the successful occlusion of the left middle cerebral artery (MCA). (c) The maximum intensity projection and volume rendering DSA images clearly show the disappearance of left MCA.

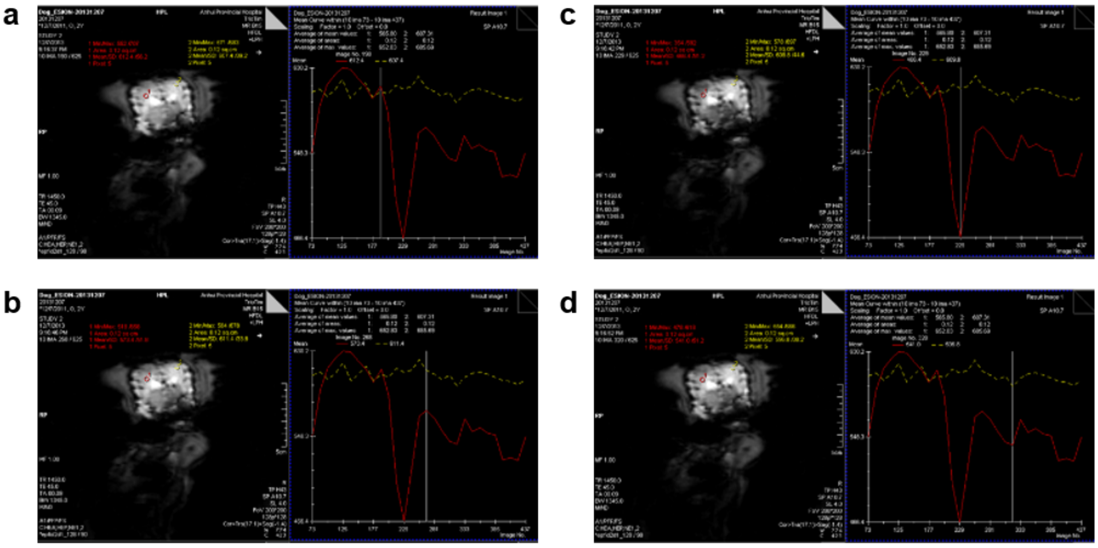

Figure S12. Perfusion weighted imaging (PWI) images at the different four time points in a dog with the left cerebral ischemia, which show more decrease in signal intensity at the normal right cerebral hemisphere (red circles and curves) than left side (yellow circles and curves).

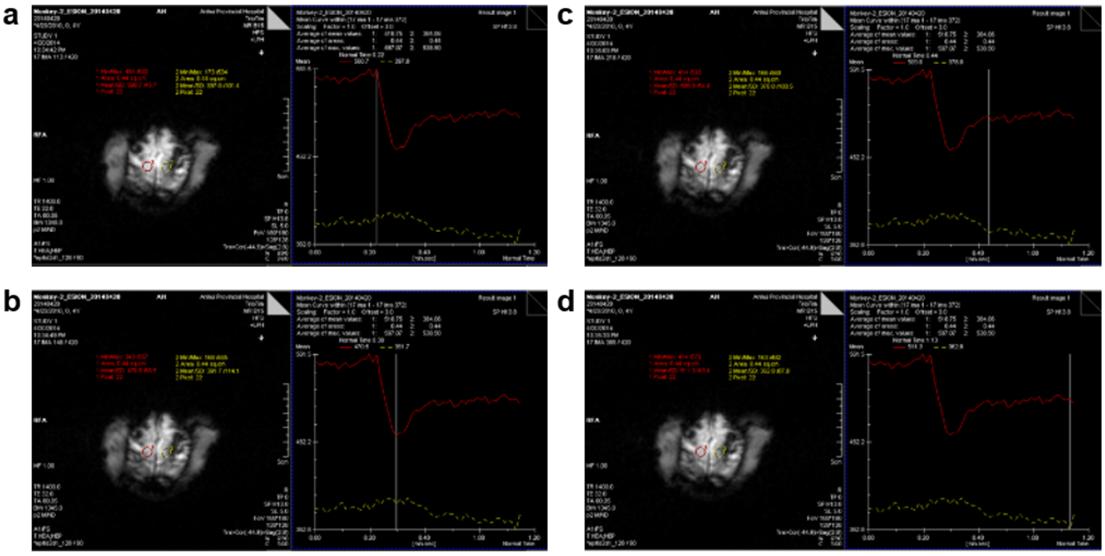

Figure S13. PWIs at the different four time points in a monkey after induction of the left cerebral ischemia, where more obvious hypointensity is present at the normal right cerebral hemisphere (red circles and curves) than left side (yellow circles and curves).